Localization and coherent dynamics of excitons in the two-dimensional optical spectrum of molecular J-aggregates

Dijkstra, Arend G.; Jansen, Thomas La Cour; Knoester, Jasper

Published in:
Journal of Chemical Physics

DOI:
10.1063/1.2897753

Publication date:
2008

Localization and coherent dynamics of excitons in the two-dimensional optical spectrum of molecular *J*-aggregates

Arend G. Dijkstra, Thomas la Cour Jansen, and Jasper Knoester[a)]
Institute for Theoretical Physics and Zernike Institute for Advanced Materials, University of Groningen, Nijenborgh 4, 9747 AG Groningen, The Netherlands

(Received 21 December 2007; accepted 21 February 2008; published online 24 April 2008)

Two-dimensional optical spectra of *J*-aggregates at low temperature provide a large amount of information about the nature and dynamics of exciton states that is hidden in conventional broad band pump-probe spectra. By using numerical simulations, we study the two-dimensional absorption spectrum and find that it is dominated by a V-shaped negative peak and a blueshifted elliptic positive peak. We demonstrate a simple method to derive the energy dependence of the exciton localization size from the distance between these two features in the zero waiting time experiment. When the waiting time is turned on, the V peak is filled with an extra positive peak resulting from population relaxation. From the time evolution of this peak, energy dependent relaxation rates can be obtained. The oscillations of coherent contributions to the two-dimensional spectrum are not damped by inhomogeneous mechanisms and can be seen clearly.
 [DOI: 10.1063/1.2897753]

I. INTRODUCTION

Recently, two-dimensional (2D) optical spectroscopy has been developed as a tool to study exciton states and relaxation in various systems.[1–9] At room temperature, 2D spectroscopy of molecular aggregates in solution has been used to study exciton delocalization lengths and relaxation rates.[1] To our knowledge, no 2D spectra of aggregates at low temperature have been reported. To obtain precise information on structure, and to study the exciton level statistics, it will be of interest to perform such studies. The liquid in which the aggregates are dissolved freezes at low temperature and the aggregates become embedded in a glassy surrounding material. Fluctuations in electronic energies due to interaction with phonons are much slower than at room temperature, and the dynamic line broadening becomes small. Slow fluctuations remain, leading to a spectral shape that is determined by static disorder. In particular, static disorder in the monomer energies plays an important role in understanding the optical properties of linear molecular *J*-aggregates.[10] At low temperature, the Frenkel exciton model combined with a static variation of site energies has been successful in explaining the linear absorption,[11,12] fluorescence,[11,13] and pump-probe spectra.[14] All these techniques probe the bulk properties of aggregates and give information averaged over a range of energies. In order to study the energy dependence of the static properties of exciton states, such as their localization length, or of the dynamic properties, such as energy relaxation and the role of coherent superpositions, one can use single molecule spectroscopy,[15–17] or frequency resolved nonlinear optical techniques.

The usefulness of 2D spectroscopy for studying dynamics originates from the possibility of measuring spectra for various waiting times. Ultrafast laser pulses first create a wavepacket in the manifold of one-exciton states. The experiment is such that during the waiting time, this wavepacket is left to evolve freely in time. The dynamical evolution of the wavepacket is reflected in the measured signal. 2D spectroscopy is therefore useful to study processes such as population relaxation and, in particular, the time evolution of coherent superpositions of exciton states. This information is typically more difficult to extract from conventional pump-probe spectra, where contributions at different energies are added to form the signal. This addition leads to inhomogeneous dephasing, the effect that coherent contributions with different frequencies cancel out.

In this paper, we study the 2D optical spectrum of linear *J*-aggregates at low temperature. We introduce a method to extract the energy dependence of the localization length from the zero waiting time spectrum. We also discuss the waiting time dependence of the low temperature spectrum and describe the clear observation of coherent contributions. The paper is organized as follows. In Sec. II, we describe the model used to study the exciton states and their dynamics at low temperature. In Sec. III, we explain the perturbative calculation of 2D spectra and consider the example of a homogeneous aggregate. In Sec. IV, we then turn to the discussion of the spectrum resulting from our model for zero waiting time and of the procedure to extract the energy dependent delocalization length from it. Sec. V, we present the calculated spectra for finite waiting time and the observation of coherent oscillations. In Sec. VI, we discuss the limitations of our approach. In Sec. VII, we present our conclusion.

II. MODEL

A. Aggregates

The Frenkel exciton Hamiltonian that describes linear *J*-aggregates at low temperature is given by

[a)]Electronic mail: j.knoester@rug.nl.

$$H = \sum_n \epsilon_n c_n^\dagger c_n + \sum_{m \neq n} \frac{-J}{|n-m|^3} c_n^\dagger c_m. \quad (1)$$

Each monomer is modeled as a two-level system and labeled by an index n. It has an excitation energy ϵ_n, and its creation and annihilation operators are denoted by $c_n^\dagger$ and c_n. The electronic excitations are paulions, which means that they behave as bosons when they are on different sites, but two excitations on the same monomer cannot occur. Therefore, the commutation relations for their operators are given by $[c_m, c_n^\dagger] = \delta_{mn}(1 - 2c_n^\dagger c_n)$. Static disorder, resulting from slow or frozen fluctuations in the environment, is introduced in the model by treating the monomer energies as independent Gaussian random variables with standard deviation σ. The average value is set to $\langle \epsilon \rangle = 0$ without loss of generality. The monomers are coupled by long-range dipole-dipole interactions. The strength of the interactions is determined by the parameter $-J$, which gives the coupling between two neighboring molecules. We will take J, which is positive for a J-aggregate, as the unit of energy throughout the paper. The summations in Eq. (1) are understood to run from 1 to the number of monomers N.

The eigenstates of the Hamiltonian can be classified according to the number of excitations present in the system, which is a conserved quantity. The only states that will be relevant in a perturbative description of the 2D spectroscopic experiment are the ground state and the states where one or two excitations are present. Numerical diagonalization of the Hamiltonian gives the one-exciton states $|u\rangle$ with energies E_u and wave function components $\phi_{u,n}$ (which are taken to be real numbers), such that $H|u\rangle = E_u|u\rangle$ and $|u\rangle = \Sigma_n \phi_{u,n} c_n^\dagger |0\rangle$. The two-exciton states $|w\rangle$ have energies E_w and can be expanded on the basis of direct products of monomer excitations, $|w\rangle = \Sigma_{n<m} \phi_{w,nm} c_n^\dagger c_m^\dagger |0\rangle$. When only the interactions between neighboring monomers are taken into account, the two-exciton states can be expressed analytically as antisymmetric products of one-exciton states.[18–20] In our model, long-range interactions are present, and we obtain the two-exciton energies and wave functions by numerical diagonalization as well. To reduce the amount of computer time needed for this diagonalization, we limit the number of two-exciton states included in the calculation. In principle, for an aggregate containing N monomers, there are $N(N-1)/2$ two-exciton states. However, for a J-aggregate, all exciton states with considerable oscillator strength occur at the bottom of each exciton manifold. At low temperature, only these states contribute to the spectrum. Therefore, we included only the lowest N_{2ex} states in the two-exciton manifold in our calculations. Their energies and wave functions are found using a Jacobi–Davidson algorithm.[21,22] The number of two-exciton states that need to be taken into account depends on the number of localization segments and, thus, on disorder.

In the dipole approximation, the coupling of the excitons to the electromagnetic field is described by the matrix elements of the dipole operator $\hat{\mu}$. Permanent dipole moments typically only have a small influence on electronic spectra. If they are assumed to be absent, the dipole operator always increases or decreases the number of excitations by 1. Matrix elements between the ground state and the two-exciton states are therefore zero. Transition dipoles between the ground state and a one-exciton state $|u\rangle$ are given by

$$\mu_u = \langle u|\hat{\mu}|0\rangle = \sum_n \phi_{u,n}. \quad (2)$$

We made the assumption that the transition dipoles of each monomer in the chain are equal and chose their lengths to be 1. Because all dipoles point in the same direction, their vector nature is irrelevant. Similarly, the transition dipole matrix element between a one-exciton state $|u\rangle$ and a two-exciton state $|w\rangle$ is

$$\mu_{wu} = \langle w|\hat{\mu}|u\rangle = \sum_{n<m} \phi_{w,nm}(\phi_{u,n} + \phi_{u,m}). \quad (3)$$

B. Relaxation

The description of the dynamics in the one-exciton manifold requires a model for the time evolution of populations and coherent superpositions of one-exciton states. Several time dependent processes will take place. First of all, excitons couple to the electromagnetic field through their transition dipole and, therefore, radiative decay to the ground state is possible. Radiative decay leads to an exponential decrease in exciton population. The decay rate for state u is given by the golden rule as $\mu_u^2 \gamma_0$, where γ_0 is the radiative decay constant of a monomer. In J-aggregates, decay will occur mainly from states at the bottom of the band, which have a large transition dipole to the ground state. In principle, one should take into account the possibility of a radiative decay to vibrationally excited sublevels of the electronic ground state, but such decay channels are strongly surpressed for delocalized excitons.[23] We assume that other mechanisms that remove the population from the one-exciton band are also slow compared to radiative decay and intraband dynamics.

Transitions within the one-exciton band are caused by the interaction of excitons with phonons in the host material. At low temperature, these interactions are small and the exciton states are only slightly perturbed by the phonons. The induced fluctuations lead to a relaxation of the exciton states. A perturbation theory in the exciton-phonon interaction with the Markoff and secular approximations gives a Pauli master equation for the population relaxation during t_2, which was applied successfully to explain the temperature dependent properties of J-aggregates.[11,12] The relaxation rate W_{vu} from state u to state v is given as the product of the wave function overlap between the initial and final states, the phonon spectral density F at the energy gap, and a temperature-dependent phonon occupation factor n_{ph},

$$W_{vu} = \left(\sum_n \phi_{u,n}^2 \phi_{v,n}^2 \right) F(|E_u - E_v|) n_{ph}(E_u - E_v). \quad (4)$$

In our calculations, we use a cubic spectral density, $F(\omega) = W_0(\omega/J)^3$, with a parameter W_0 that scales the overall value of the exciton phonon scattering rates. We use a value of $W_0 = 16J$, which was found in earlier work to be a typical interaction strength in linear aggregates.[12] A cubic spectral density is appropriate for scattering off low-frequency phonons; it is found from a product of the phonon density of

states, which is quadratic in frequency, and the exciton phonon coupling constant squared, which, to lowest order, is linear in frequency.[24–26] The factor n_{ph} is given as the sum of two terms, $n_{\mathrm{ph}}(\omega)=\theta(\omega)+(\exp(|\omega|/k_BT)-1)^{-1}$. The first term describes a spontaneous emission of a phonon and is 1 if $\omega>0$ and zero otherwise. The second term is the Bose–Einstein distribution at temperature T, which describes the phonon absorption and stimulated emission contributions to the relaxation rate. In this work, we set the temperature to $k_BT=0.005J$, which corresponds to 4 K for a typical J value of 500 cm^{-1}. The master equation that describes the time evolution of a population $\mathcal{P}_u$ in state $|u\rangle$ resulting from a radiative decay and an interaction with phonons is then given by

$$\frac{d}{dt}\mathcal{P}_u(t)=\sum_v (W_{uv}\mathcal{P}_v(t)-W_{vu}\mathcal{P}_u(t))-\gamma_0\mu_u^2\mathcal{P}_u(t). \tag{5}$$

At the same level of theory, coherent superpositions of one-exciton states undergo damped oscillations during the waiting time. The oscillation frequency is determined by the energy difference of the two states in the superposition, and the damping constant γ follows from the relaxation rates,[27]

$$\gamma_{uv}=\gamma_{u0}+\gamma_{v0}, \tag{6}$$

with

$$\gamma_{u0}=\tfrac{1}{2}\sum_p (W_{pu})+\tfrac{1}{2}\gamma_0\mu_u^2. \tag{7}$$

III. 2D SPECTROSCOPY

A 2D spectrum displays information gathered in a nonlinear optical experiment.[28] Three ultrashort laser pulses with different wave vector are used to selectively study third-order nonlinear processes. The short pulse duration corresponds to a bandwidth that is large enough to excite all states in the J band coherently. In general, pulse polarization can be used as an additional tool to select specific processes, but in an aggregate where all dipoles are parallel, polarization is not important. The first pulse brings the system into a coherent superposition of the ground state and a state in the one-exciton manifold. This state evolves for a time t_1, after which the second pulse interacts and creates a population in the ground state, a population in a one-exciton state, or a coherence between two one-exciton states. After a waiting time t_2 and the interaction with the third pulse, coherences between the ground state and a one-exciton state or between a one-exciton state and a two-exciton state are excited. These coherences evolve during a time t_3. A signal is then detected. The 2D spectrum displays the obtained information in the frequency domain. The oscillation frequency ω_1 of the system during t_1 is displayed on the horizontal axis, while the vertical axis shows the frequency ω_3 during t_3. The displayed signal, thus, is a map correlating the initial frequency ω_1 with the frequency ω_3 after a waiting time t_2. Experimentally, the spectrum along the ω_1 direction is most commonly obtained by recording the response for various values of t_1 and performing a Fourier transform. The emitted signal is typically frequency resolved to obtain the spectrum as a function of ω_3. In this approach, as in other methods used to collect a 2D spectrum, short pulses with a corresponding large bandwidth are used. Many exciton states are therefore excited coherently. Nevertheless, it is often convenient to describe ω_1 and ω_3 simply as "pump" and "probe" frequencies, respectively. As long as coherent superpositions of one-exciton states during t_2 are properly taken into account, the total spectrum can then be interpreted as a sum of many narrow band pump-probe experiments.

As long as the size of the sample that is probed is much larger than the wavelength of the applied light, a signal is detected only in specific directions. Two directions are important for 2D spectroscopy, the $\mathbf{k}_{\mathrm{I}}=-\mathbf{k}_1+\mathbf{k}_2+\mathbf{k}_3$ (rephasing) direction and the $\mathbf{k}_{\mathrm{II}}=\mathbf{k}_1-\mathbf{k}_2+\mathbf{k}_3$ (nonrephasing) direction ($\mathbf{k}_i$ denotes the wave vector of pulse i). The signals in the $\mathbf{k}_{\mathrm{I}}$ and $\mathbf{k}_{\mathrm{II}}$ directions result from pathways where, during t_2, the system is in a population of a one-exciton state, in a coherent superposition of two different states from the one-exciton manifold, or in the ground state. These signals are therefore useful to study t_2 dependent processes in the one-exciton manifold. In principle, a third independent detection direction $\mathbf{k}_{\mathrm{III}}=\mathbf{k}_1+\mathbf{k}_2-\mathbf{k}_3$ exists. In this case, the system is in a coherent superposition of the ground state and a two-exciton state during t_2. In the limit of short pulses, the $\mathbf{k}_{\mathrm{III}}$ signal does not mix with the $\mathbf{k}_{\mathrm{I}}$ and $\mathbf{k}_{\mathrm{II}}$ signals, and as we are currently not interested in the dynamics of coherences between the two-exciton states and the ground state, we will not study the $\mathbf{k}_{\mathrm{III}}$ contribution. Processes detected in the rephasing ($\mathbf{k}_{\mathrm{I}}$) direction radiate a photon echo signal. In this case, the specific sequence of interactions between the system and the light gives rise to macroscopic rephasing and, at time $t_3=t_1$, all dipoles in the system oscillate in phase and produce the echo. For low intensity ultrashort pulses, the response from these processes can be calculated from third-order response theory in the rotating wave approximation to be[29,30]

$$\begin{aligned}
S_I(\omega_1,t_2,\omega_3)=&-\left\langle\sum_{u,u'}\mu_u^2\mu_{u'}^2\mathcal{P}_{1\mathrm{ex}}(t_2)\delta(\omega_1+E_u)\delta(\omega_3-E_{u'})\right\rangle\\
&-\left\langle\sum_{u,u'}\mu_u^2\mu_{u'}^2P_{u'u}(t_2)\delta(\omega_1+E_u)\delta(\omega_3-E_{u'})\right\rangle\\
&+\left\langle\sum_{u,u',w}\mu_u^2\mu_{wu'}^2P_{u'u}(t_2)\delta(\omega_1+E_u)\delta(\omega_3-E_{wu'})\right\rangle\\
&-\left\langle\sum_{v\neq u}\mu_u^2\mu_v^2e^{(-i\omega_{vu}-\gamma_{vu})t_2}\delta(\omega_1+E_u)\delta(\omega_3-E_v)\right\rangle\\
&+\left\langle\sum_{v\neq u,w}\mu_u\mu_v\mu_{wv}\mu_{wu}e^{(-i\omega_{vu}-\gamma_{vu})t_2}\delta(\omega_1+E_u)\right.\\
&\left.\times\delta(\omega_3-E_{wu})\right\rangle.
\end{aligned} \tag{8}$$

The first term in this equation describes the bleaching signal. It is proportional to the total population in one-exciton states $\mathcal{P}_{1\mathrm{ex}}(t)=\Sigma_u\mathcal{P}_u(t)$. The second term describes stimulated emission pathways, and the third one an absorption into a two-exciton state. During t_2, the system is in a population in a one-exciton state. Population relaxation can occur, which is described by the conditional probability $P_{u'u}(t)$ that a popu-

lation in state $|u\rangle$ at $t=0$ has been transferred to state $|u'\rangle$ at time t. $P_{u'u}(t)$ is obtained as the solution to Eq. (5), $P_{u'u}(t)=(\exp(Rt))_{u'u}$ with $R_{u'u}=(1-\delta_{u'u})W_{u'u}-2\delta_{u'u}\gamma_{u0}$. The last two terms in Eq. (8) describe stimulated emission and induced absorption processes, where a coherent superposition of one-exciton states exists during t_2. This coherent superposition oscillates with a characteristic frequency $\omega_{vu}=E_v-E_u$ and is damped with damping constant γ_{vu} [Eq. (6)]. Nonrephasing $\mathbf{k}_{\mathrm{II}}$ processes, for which the phase evolution during t_1 and t_3 occurs with the same sign, give a similar signal,

$$
\begin{aligned}
S_{II}(\omega_1,t_2,\omega_3) &= -\left\langle \sum_{u,u'} \mu_u^2\mu_{u'}^2 \mathcal{P}_{1\mathrm{ex}}(t_2)\,\delta(\omega_1-E_u)\,\delta(\omega_3-E_{u'})\right\rangle \\
&\quad -\left\langle \sum_{u,u'} \mu_u^2\mu_{u'}^2 P_{u'u}(t_2)\,\delta(\omega_1-E_u)\,\delta(\omega_3-E_{u'})\right\rangle \\
&\quad +\left\langle \sum_{u,u',w} \mu_u^2\mu_{wu'}^2 P_{u'u}(t_2)\,\delta(\omega_1-E_u)\,\delta(\omega_3-E_{wu'})\right\rangle \\
&\quad -\left\langle \sum_{v\neq u} \mu_u^2\mu_v^2 e^{(-i\omega_{uv}-\gamma_{uv})t_2}\,\delta(\omega_1-E_u)\,\delta(\omega_3-E_u)\right\rangle \\
&\quad +\left\langle \sum_{v\neq u,w} \mu_u\mu_v\mu_{wv}\mu_{wu} e^{(-i\omega_{uv}-\gamma_{uv})t_2}\,\delta(\omega_1-E_u) \right. \\
&\quad \left. \times\,\delta(\omega_3-E_{wv})\right\rangle. \qquad (9)
\end{aligned}
$$

The 2D correlation spectrum is defined as the sum of the rephasing and nonrephasing spectra. This combination eliminates most of the phase twist that is present in the individual spectra.[31,32] After a convolution (denoted $*$) with a 2D Lorentzian line shape to account for homogeneous broadening, the correlation spectrum is given by

$$
\begin{aligned}
S(\omega_1,t_2,\omega_3) = \mathrm{Re}\Bigg(& S_I(-\omega_1,t_2,\omega_3) * \frac{1}{\omega_1-i\gamma}\frac{1}{\omega_3+i\gamma} \\
& + S_{II}(\omega_1,t_2,\omega_3) * \frac{-1}{\omega_1+i\gamma}\frac{1}{\omega_3+i\gamma}\Bigg). \qquad (10)
\end{aligned}
$$

Here, we assume that the homogeneous broadening γ does not vary with energy.

As an example of the 2D spectrum that will help in the interpretation of the spectra of disordered aggregates, we treat the homogeneous aggregate at zero waiting time ($t_2=0$). In this case, all monomer transition energies are equal, $\epsilon_n=\langle\epsilon\rangle=0$. We further simplify the model by taking into account only interactions between neighboring monomers. The energies of one- and two-exciton states and the transition dipoles connecting the ground state with the one-exciton states and the one-exciton states with the two-exciton states can be obtained analytically in this model. Briefly, the one-exciton states have energies $E_u/J=-2\cos[u\pi/(N+1)]$ ($u=1,2,\ldots,N$). Bright states are the states with odd u at the bottom of the band. In particular, the oscillator strength of the lowest ($u=1$) state is found to be $0.81N$ and the oscillator strength of the $u=3$ state is $0.09N$. Together, these two transitions account for most of the total oscillator strength of the one-exciton band, which is equal to N. Because under the assumption of nearest-neighbor interactions the excitons behave as noninteracting fermions, the two-exciton states are found as antisymmetric products of two different one-exciton states;[18–20] the transition dipoles connecting them with the one-exciton states are given in Ref. 33. We label the two-exciton states as $|w\rangle=|u1,u2\rangle$, where $|u1\rangle$ and $|u2\rangle$ are two different one-exciton states. The most intense transition from the one- to the two-exciton band is found between the $|1\rangle$ and $|1,2\rangle$ states and has an oscillator strength of $1.27N$.

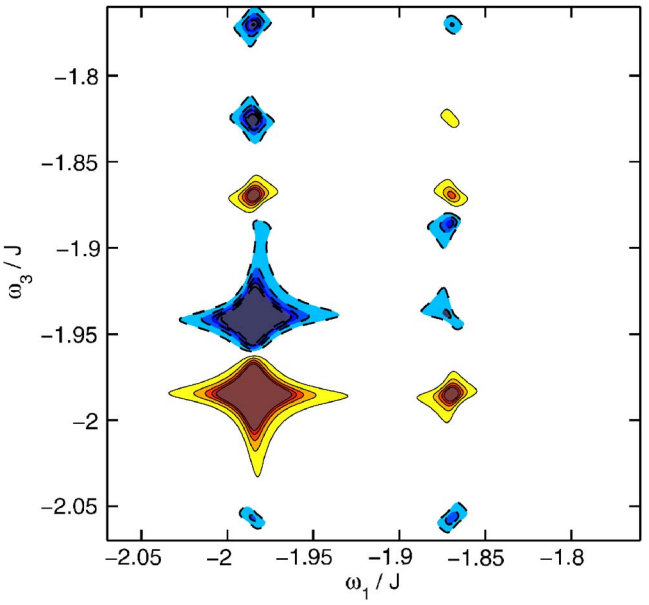

FIG. 1. (Color online) 2D correlation spectrum for a 25 monomer homogeneous aggregate with nearest-neighbor interactions only. The homogeneous linewidth is $\gamma=0.005J$ and contours are drawn at $\pm1\%$, 2%, 3%, 4%, and 5% of the peak maximum. The contours in negative peaks are drawn as solid lines, dashed lines indicate positive peaks.

In the 2D correlation spectrum calculated from this model with $N=25$, shown in Fig. 1, we see negative bleaching and stimulated emission peaks (color coded in red) and positive induced absorption peaks (color coded in blue). Negative peaks are seen on the diagonal at energies $\omega_1=\omega_3=E_1=-1.985J$ and at $\omega_1=\omega_3=E_3=-1.870J$. Additional negative peaks are seen off the diagonal. The presence of these cross peaks reveals the overlap of exciton wave functions.[34] For nonoverlapping one-exciton states, the 2D response consists of diagonal negative (bleaching and stimulated emission) contributions only. This can be understood from the physics of the experiment. For each frequency during t_1, represented by a vertical slice through the 2D spectrum, the pump pulse will populate one-exciton states with a certain energy. For nonoverlapping states (and no exciton-exciton interaction), this does not influence the probe absorption in any state except the ones that are pumped. The difference signal that is plotted is therefore zero except when the probe frequency is equal to the pump frequency. The statement that nonoverlapping states produce only a diagonal negative peak can also be seen from the derivation of the nonlinear response. If two one-exciton states $|u_1\rangle$ and $|u_2\rangle$ do not overlap, their direct product state is also an eigenstates of the Hamiltonian. The direct product forms the two-exciton state, in which both $|u_1\rangle$ and $|u_2\rangle$ are excited. It has an energy $E_{u1}+E_{u2}$, and the transition dipole connecting the direct product

state with $|u_1\rangle$ is equal to the transition dipole between $|u_2\rangle$ and the ground state. Using these properties in Eq. (8), one observes that the induced absorption and the off-diagonal bleaching contributions to the spectrum exactly cancel each other. The rephasing response then reduces to

$$S_I(\omega_1,t_2=0,\omega_3)=-2\left\langle \sum_u \mu_u^4 \delta(-\omega_1-E_u)\delta(\omega_3-E_u)\right\rangle, \tag{11}$$

and, indeed, the signal is negative everywhere and appears on the $\omega_1=\omega_3$ diagonal. The presence of negative peaks off the diagonal (cross peaks) and of positive peaks, therefore, gives information on the overlap of exciton states. Apart from these clear negative diagonal and cross peaks, a final negative peak appears just above the $u=3$ diagonal peak, which originates in a nonrephasing pathway with a coherent superposition of the $u=3$ and $u=1$ states during t_2 and of the $|2,3\rangle$ two-exciton state with the $u=1$ state during t_3.

Positive peaks show absorption into the two-exciton manifold. The most intense peak, which appears above the $u=1$ diagonal peak at $(\omega_1,\omega_3)=(E_1,E_2)$, results from an excitation of the $|1,2\rangle$ two-exciton state. The two other strong induced absorption peaks at $\omega_1=E_1$ show an excitation of the $|2,3\rangle$ and $|1,4\rangle$ two-quantum states. The intensity in these peaks is the sum of contributions from pathways with a population during t_2 and pathways with a coherence during t_2. In addition, peaks are present in the spectrum that result from coherent contributions. In particular, the two peaks at the bottom of the spectrum ($\omega_3=-2.057J$) are mainly coherent.[27]

The line shape in the homogeneous case is a 2D Lorentzian. In the peaks that result from pathways with a coherence during t_2, the effect of an imperfect balance of rephasing and nonrephasing pathways is seen as a residual phase twist.

IV. STATIC SPECTRA AND LOCALIZATION

We now turn to the more general case, where long-range dipole dipole interactions and disorder in the site energies are taken into account. We will first describe the spectrum for zero waiting time, $t_2=0$, and discuss the origin of the peaks in terms of localized exciton states. The 2D correlation spectrum calculated for a chain with 100 monomers and a diagonal disorder of $\sigma=0.2J$ is shown in Fig. 2. As described in Sec. II, only the lowest two-exciton states are taken into account. We set $N_{2ex}=30$ and checked that the spectra do not change significantly when this number is increased. The main features in the 2D spectrum are a negative peak with a tilted V shape and a positive elliptic peak with a long axis parallel to the diagonal. The left leg of the V-shaped peak is a narrow strong signal on the $\omega_1=\omega_3$ diagonal line. Apart from coherent contributions from nonrephasing pathways, this diagonal feature is the result of bleaching and stimulated emission processes involving only a single one-exciton state. Its elongation along the diagonal is a signal of the strong inhomogeneous broadening, because the diagonal intensity reflects the distribution of exciton energies weighed by their dipole to the fourth power. The inhomogeneous broadening

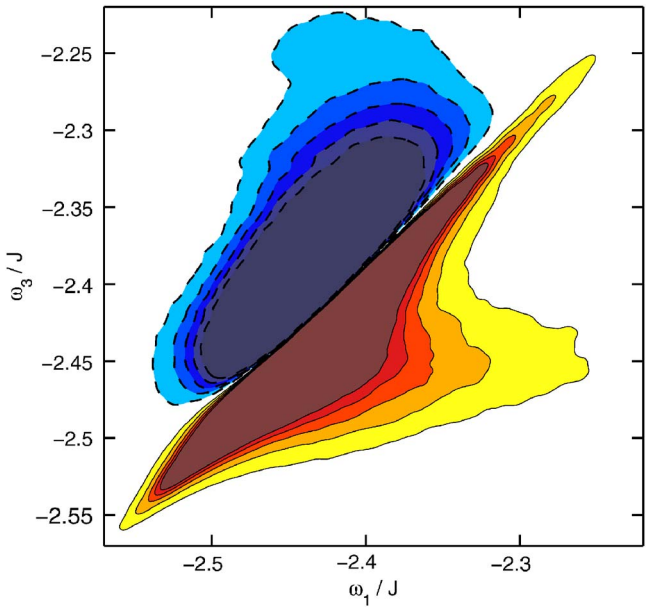

FIG. 2. (Color online) 2D correlation spectrum for a 100 monomer inhomogeneous aggregate at zero waiting time. The standard deviation of the diagonal disorder is $\sigma=0.2J$. The homogeneous linewidth is $\gamma=0.005J$. The spectrum is normalized to its maximum amplitude and contours are drawn at $\pm 1\%$, 2%, 3%, 4%, and 5% of this maximum.

does not influence the antidiagonal width of the peak, which is only due to homogeneous broadening mechanisms. In our simulations, we used a uniform homogeneous linewidth $\gamma=0.005J$, which gives rise to the narrow antidiagonal width seen at the blue side of the negative peak. The very narrow homogeneous width can only be observed at low temperature. At higher temperatures, thermal dephasing leads to an extra homogeneous broadening, causing the diagonal signal to broaden in the antidiagonal direction, most strongly at the high frequency side. As a result, the two legs of the V will overlap and the V shape will not be observable at high temperature.

At the low temperature used in Fig. 2, the lower frequency part of the diagonal peak appears to have a larger antidiagonal width than the high-frequency side. This is caused by an overlap with the right leg of the V shape, a cross peak extending almost horizontally in the ω_1 direction. This negative cross peak is the result of bleaching and stimulated emission pathways that involve two different one-exciton states. At a given point (ω_1,ω_3) in the spectrum, the first pulse interacts with an exciton state that has an energy ω_1, while the third pulse probes a state with energy ω_3. The cross peak is strongest when a state with a large transition dipole to the ground state is probed. Such states are by definition most abundant in the center of the *J*-band (which is found at the bottom of the exciton band), and the cross peak forms for values of ω_3 in the middle of this band. The observation of the cross peak means that these two exciton states must be overlapping in space, because a pair of nonoverlapping exciton states does not give a contribution to the cross peak (see Sec. III). The existence of overlapping states is also apparent from the positive elliptic peak that is seen above the negative V peak. This peak shows the signal from induced absorption pathways, where two-exciton states are

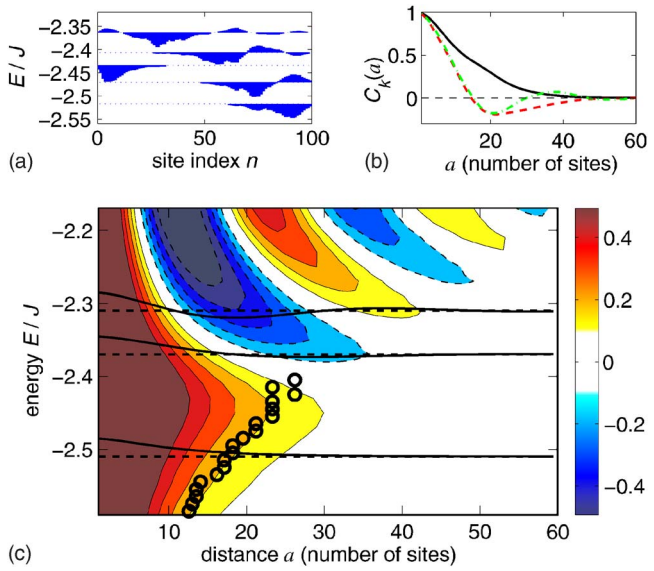

FIG. 3. (Color online) (a) displays the five lowest wave functions in a 100 monomer chain offset by their energy, for a single realization of the disorder. The first, second, and fourth states from the bottom of the band form a localization segment on the right hand side of the chain. (b) shows the correlation functions for these states, drawn with a solid line, a dashed line, and a dash-dotted line, respectively. The correlation function $C(a;E)$ averaged over 100 000 realizations of the disorder is shown in (c). The diagonal disorder is sampled from a Gaussian distribution and has a standard deviation of $\sigma=0.2J$. Contours are drawn at ± 0.1, 0.2, 0.3, 0.4, and 0.5. The solid lines show the correlation function at a single energy. The circles show the length extracted from the peak splitting in the 2D spectrum.

excited during t_3. We note that other positive peaks are present in the spectrum with a very low intensity. In particular, the coherent peak described in Ref. 27 is also present in our current calculation, but its amplitude is too small to be seen with the chosen contours.

To analyze the peaks that are observed in the 2D spectrum in more detail, we need to consider the properties of the exciton states that are interacting with light. In a *J*-aggregate, all states with oscillator strength are found at the bottom of the band. As a result of disorder, each low-lying exciton state is localized on a part of the chain. If one calculates the wave functions of these localized states, it is found that, at the bottom of the band, most wave functions look like the $|u=1\rangle$ state in the homogeneous aggregate.[35,13,36] These states are called *S* states and carry most of the oscillator strength of the chain. In the homogeneous aggregate, the $|u=1\rangle$ state has no nodes in the wave function. Likewise, *S* states are defined as states where almost all amplitudes of the wave function are found in a contiguous segment, where the wave function does not change sign. The typical size of such a segment, N^*, is given by the delocalization size of the *S* state. The similarity between *S* states and $|u=1\rangle$ states suggests the interpretation of a localization segment as a homogeneous chain with length N^*. It is then natural to look for *P* states, which, in analogy to the $|u=2\rangle$ state, have a node that separates a predominantly positive region from a predominantly negative region of the wave function. Such *P* states can, indeed, be found.[35] An example of a localization segment is given in Fig. 3(a), where the two lowest-energy states on the right side of the chain form an *SP* pair. The correspondence between the homogeneous chain and a localization segment is not exact, as we stress by using different notations in the two cases. In particular, *P* states are generally not completely antisymmetric and, therefore, have a nonvanishing oscillator strength. However, it is still useful to interpret the nonlinear optical response in terms of *S* and *P* states.

The diagonal peak is then caused mainly by bleaching and stimulated emission of *S* states. These states carry most oscillator strength and, therefore, explain a large part of the linear response. In the diagonal peak of the 2D spectrum, contributions from non-*S* states are even smaller, because the amplitude of this peak scales as the oscillator strength squared. However, small contributions of *P* states and of higher-lying states are present at the high energy side of the *J*-band. The negative cross peak below the $\omega_1=\omega_3$ diagonal has contributions from the overlap of *S* states with higher lying states on the same segment and from pairs of *S* states that are localized on slightly overlapping segments. Apart from small contributions where a coherent superposition of two one-exciton states is present during t_2, the intense induced absorption peak in the 2D spectrum is caused by pathways with an *S* state during t_1 and an *SP* two-exciton state during t_3. The peak thus reflects the conditional probability of finding such a two-exciton state on a segment at energy $\omega_1+\omega_3$, given that it contains an *S* one-exciton state at energy ω_1. We stress that the identification of the two-exciton state as the state in which the *S* and *P* one-exciton states are occupied holds only in the fermion picture, i.e., in the case of nearest-neighbor interactions (Sec. III). Because we include long-range interactions, this two-exciton state is not an exact eigenstate of the Hamiltonian. Nevertheless, we will refer to the relevant two-exciton state as *SP*, because this identification still holds approximately and the use of this fermion language facilitates the interpretation of the spectra.

The properties of the localized exciton states can be studied by introducing the spatial correlation function,

$$C(a;E)=\frac{\langle \Sigma_u \Sigma_n \phi_{u,n}\phi_{u,n+a}\delta(E-E_u)\rangle}{\langle \Sigma_u \delta(E-E_u)\rangle}. \tag{12}$$

This function describes the correlation between the components of the wave function on sites that are a distance *a* apart. The correlation is evaluated at a certain energy *E* and averaged over disorder, which is implied by the notation $\langle\cdots\rangle$. The correlation function is normalized by the density of states. For a single wave function with energy E_u, the correlation function is nonzero only at $E=E_u$. It is normalized by its value at zero distance, $C(a=0;E_u)=1$, and falls off to zero on a length scale equal to the localization length. The number of nodes in the correlation function is equal to the number of nodes in the wave function. This makes it possible to infer the nature of the state (number of nodes and localization length) from the correlation function. Because the correlation function averages wave functions that are localized on different segments of the chain, it is a suitable measure to obtain statistical information on the type of exciton states that dominate at a certain energy and of their localization lengths. Other measures used to describe exciton localization, such as the inverse participation ratio calculated from different distributions,[37,38] or the absolute value correlation

function do not provide such information. The correlation function for $\sigma=0.2J$ is shown in Fig. 3.

The wave function, and therefore also the correlation function, of an *S* state contains no significant nodes. We observe from Fig. 3 that for our choice of parameters, the *S* states appear mostly below $E=-2.38J$. Their localization length increases with energy, as can be seen from the slope of the contours in the correlation function. The fact that the localization length is energy dependent is not surprising and well known.[10,39] However, with the commonly used procedure to extract the localization length from the peak splitting in the pump-probe spectrum, a single number is obtained.[19,37,40–43] It reflects the average localization size of states in the *J*-band. Surprisingly, studies of the energy dependence of the peak splitting using two-color pump-probe spectroscopy found no correlation between the peak splitting and the pump frequency, both experimentally and in simulation.[41,44,45] From this, the conclusion is that the delocalization length is independent of energy. However, as we have seen from Fig. 3, this conclusion is not consistent with the predictions of the Frenkel exciton model with diagonal disorder. Proposals to study the energy dependence have been made before, in particular, from the time dependence of the antidiagonal width of the absolute-value 2D spectrum.[1]

We present a more direct method to extract the delocalization length from the 2D spectrum at zero waiting time. In the spectrum, the distance Δ between the maximum of the bleaching peak and the maximum of the induced absorption is measured in a slice at a fixed value of $\omega_1=E$. In such a slice, only one-exciton states with an energy *E* are excited by the pump beam. Δ measures the energy separation between these states and a higher-lying state on the same segment. In the same way as in the broadband pump-probe spectrum, this separation depends on the size of the segment. From the distance Δ, the delocalization length at energy *E* can therefore be extracted using the relation[45]

$$N^*(E) = \pi \sqrt{\frac{3J}{\Delta(\omega_1 = E)}} - 1. \tag{13}$$

This definition assumes that the excitons that are probed resemble the states in a homogeneous system with length N^*, where only nearest-neighbor interactions are present. The induced absorption peak comes from an excitation of the *SP* ($|1,2\rangle$) two-exciton state, which is separated along ω_3 from the *S* ($|u=1\rangle$) bleaching and stimulated emission peak by a distance $\Delta=E_2\approx 3\pi^2 J/(N^*+1)^2$. Repeating the procedure for different values of ω_1 then gives the energy dependent delocalization length. With this method, it is possible to obtain the length from a single spectrum as long as the homogeneous linewidth is small. In order to demonstrate the method, we have applied it to the calculated spectrum shown in Fig. 2. The extracted energy dependent delocalization length is shown in Fig. 3 as circles. We observe a clear energy dependence, and the extracted localization size nicely follows the 0.2 contour of the correlation function. The localization length that is extracted from the spectrum thus agrees well with the localization properties found in a direct simulation, even though the extraction procedure relies on the approximation of nearest-neighbor interactions. We conclude that 2D spectroscopy might be used to measure the energy dependent delocalization length at low temperatures.

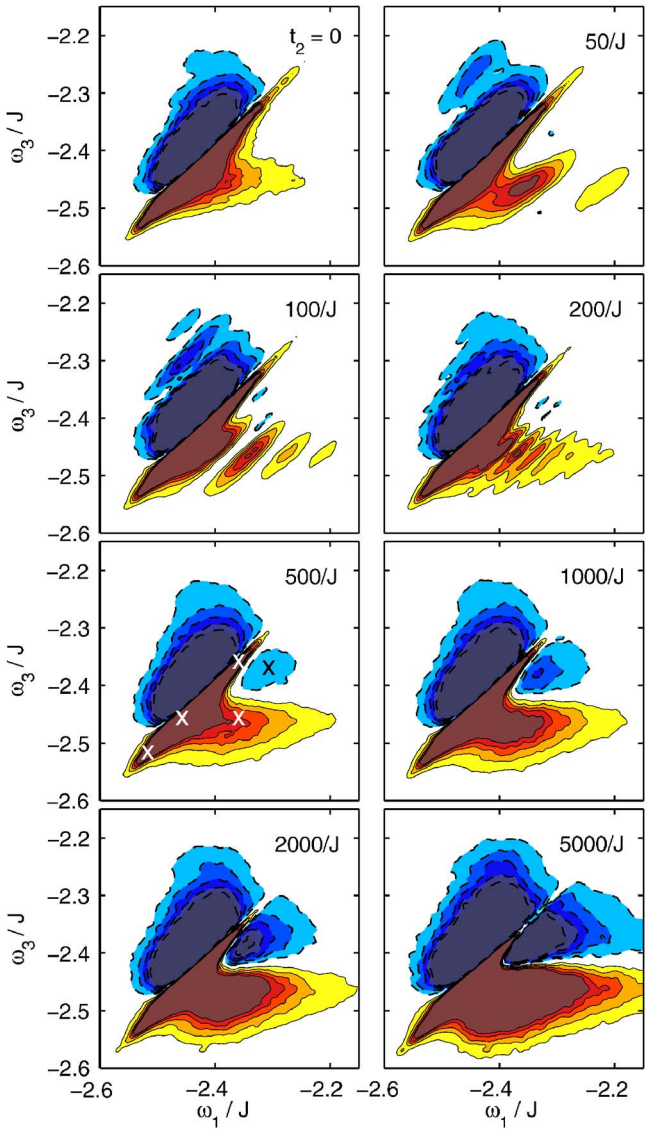

FIG. 4. (Color online) 2D correlation spectra for various waiting times. The static parameters are the same as in Fig. 2. The strength of the exciton phonon coupling is $W_0=16J$, the radiative lifetime of a monomer is $\gamma_0=1.5\times10^{-5}J$, and the temperature is $k_BT=0.005J$. The spectra are averaged over 8000 disorder realizations. All spectra are normalized to their maximum amplitude and contours are drawn at $\pm1\%$, 2%, 3%, 4%, and 5% of this maximum. The crosses in the $t_2=500/J$ spectrum indicate the positions where time traces shown in Figs. 5 and 6 are taken. A waiting time of $500/J$ corresponds to 33 ps for $J=500$ cm^{-1}.

V. DYNAMICS

The waiting time dependent 2D spectra can be used to study fast dynamical processes in the one-exciton band. The spectrum contains information about the evolution of a wavepacket in the one-exciton band during the waiting time. In the secular approximation, the time evolution of the wavepacket can be described as population relaxation together with damped oscillations of coherent superpositions of exciton states. The results of population relaxation are clearly observed in our calculated 2D spectra, shown in Fig. 4. The

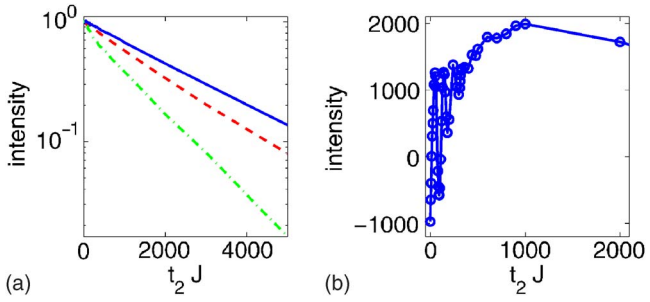

FIG. 5. (Color online) Time traces (a) in the diagonal peak at $(\omega_1,\omega_3)=(-2.53J,-2.53J)$ (solid line), $(-2.50J,-2.50J)$ (dashed line), and $(-2.47J,-2.47J)$ (dash-dotted line) and (b) in the cross peak at $(\omega_1,\omega_3)=(-2.32J,-2.38J)$. The points where the traces are taken are marked in Fig. 4 with white crosses. Note the logarithmic scale in (a).

main effects in the spectrum are an increase of the intensity of the cross peak compared to the diagonal peak and the appearance of an extra induced absorption peak that fills the V shape. At waiting times below $500/J$ (which corresponds to 33 ps for a typical value of $J=500$ cm^{-1}), coherent effects are observed.

We first turn to the waiting time dependence of the diagonal peak intensity. At low temperature, a relaxation upward in energy is very slow. The low energy side of the diagonal peak is therefore mainly influenced by the radiative decay to the ground state. Thus, in our model, the amplitude of each contribution to the diagonal peak decays exponentially with a decay constant $|\mu_u|^2\gamma_0$. Because the decay constant includes the transition dipole, it is energy dependent. As long as the distribution of dipole moments at a given energy is sufficiently narrow, the diagonal peak intensity will decay exponentially, as is, indeed, seen in the time traces for different points in the diagonal peak in Fig. 5(a). Because the dipole scales with the delocalization length as $\sqrt{N^*}$, the decay constant increases with energy for S states. This increase is clear from the figure.

In addition, the diagonal peak intensity decreases because of intraband population relaxation, governed by Eq. (5). For S states at low temperature, this relaxation is very slow. Because of the small thermal energy, relaxation within the typical localization segment, where all states have an energy larger than the energy of the S state, is suppressed. Relaxation to S states on other segments, which can be favorable energetically, is also slow, because of the small overlap between states localized on different segments.[13] We note that the decay of diagonal peaks is not completely monotonous due to the coherent contributions to the nonrephasing diagrams. These pathways give a small oscillating contribution to the amplitude.

Cross peaks show an even richer time dependent behavior. Three effects contribute to the evolution. All these effects are clearly observed in the calculated spectra. As in the case of the diagonal peak, the cross peak amplitude decreases because of a radiative decay to the ground state. Second, population relaxation generally increases the amplitude of cross peaks. Finally, coherent contributions to the cross peak give rise to damped oscillations of the amplitude. We first turn to the extra induced absorption peak that fills the V shape in the spectrum. We call this peak the *DSP* peak, because in terms of the segment model, it involves the D, S, and P states. This peak is marked in Fig. 4 (panel $t_2=500/J$) with a black cross. It grows in intensity during the waiting time, which reveals that it is caused by relaxation. If we want to interpret the *DSP* peak in terms of the segment model within the fermion approximation (Sec. III), three states are needed. During t_3, the system must be in a coherent superposition of a one- and a two-exciton state to form a positive peak. This superposition is formed between an S state and an SP two-exciton state. The position of the peak along ω_3 is then equal to the energy of the P state. The fact that the peak appears below the diagonal tells us that the state that is initially pumped has a higher energy than the P state and could be called a D state. During the waiting time, intraband relaxation takes place from this D state to the S state. If we push the comparison with the homogeneous aggregate even further, the initially pumped D state must be the $|u=3\rangle$ state. However, such a conclusion would be an overinterpretation of the segment model.

The time evolution of the *DSP* peak, obtained by taking a time trace at $(\omega_1,\omega_3)=(-2.32J,-2.38J)$, is shown in Fig. 5(b). At short times, a negative cross peak is found at these frequencies. The positive contribution from population relaxation quickly takes over and makes the total peak positive. At times larger than $1000/J$, relaxation to the ground state becomes the dominant process and the amplitude of the peak starts to decrease. However, the intensity of the diagonal peak decreases faster and the relaxation induced peak continues to get more intense relative to the diagonal. This can be seen in the normalized spectra in Fig. 4. The time evolution of coherent contributions to the peak is clearly seen from the oscillating behavior in the trace at short times. Such oscillating contributions from coherences, which were described in the electronic spectra of a dimer in Ref. 46 and in the photosynthetic complexes of bacteria in Ref. 2, can be analyzed in more detail in the cross peak region below the diagonal. Here, oscillating peaks arise from rephasing stimulated emission contributions. Pathways with a coherent superposition of two states that are separated in energy by an amount ΔE during t_2 only contribute to the spectrum at positions (ω_1,ω_3) if $|\omega_1-\omega_3|=\Delta E$. This means that the time trace at a given point in the spectrum will show oscillations with a predictable period $T_{\mathrm{osc}}=2\pi/|\omega_1-\omega_3|$. Furthermore, because no interference between different frequencies can take place, inhomogeneous dephasing is absent if the frequency resolution in the spectrum is large enough. Indeed, a time trace taken at $(\omega_1,\omega_3)=(-2.37J,-2.47J)$ (Fig. 6) shows oscillations with a period between $T_{\mathrm{osc}}=60/J$ and $T_{\mathrm{osc}}=70/J$, which is consistent with the expected value of $2\pi/|\omega_1-\omega_3|=63/J$.

Another coherent effect is seen in the spectra at $t_2=50/J$, $100/J$, and $200/J$. Separate cross peaks seem to appear, and the scale of the separation decreases with increasing waiting time. The peaks are caused by the different oscillation frequencies of coherent contributions at different parts of the spectrum. The coherent contribution oscillates as $\exp(-i\Delta E t_2)$. For a fixed value of t_2, one therefore observes an oscillating contribution to the spectrum with a frequency

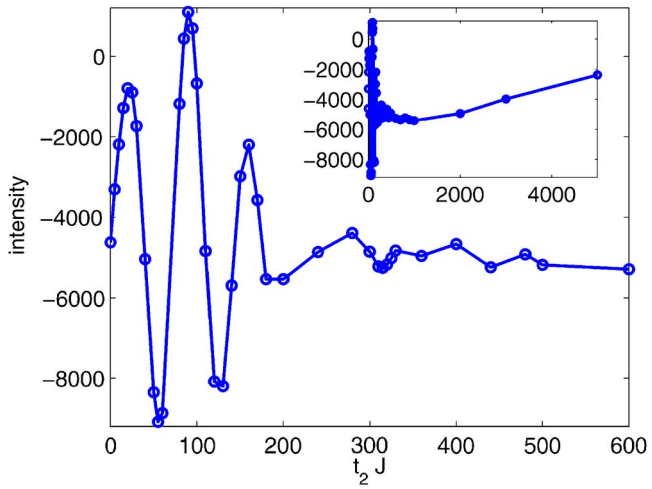

FIG. 6. (Color online) Time trace in the cross peak at $(\omega_1,\omega_3)=(-2.37J, -2.47J)$, marked in Fig. 4 with a white cross. The inset shows the trace for longer t_2.

scale dictated by the waiting time. The effect will only occur if an inhomogeneous distribution of frequencies is present in the system. Moreover, an observation of the effect is only possible if the thermal dephasing is small, that is, at low temperature.

If we naively interpret the oscillations as the time evolution of a coherent superposition of $|u=1\rangle$ and $|u=3\rangle$ states in a homogeneous aggregate with length N^* (again neglecting non-nearest-neighbor interactions), we find that the oscillation period $T_{\mathrm{osc}}=2\pi/(E_3-E_1)\approx(N^*+1)^2/4\pi J$ implies a value of $N^*=27$ at these energies. From Fig. 3, we observe that the effective delocalization size obtained here corresponds reasonably well to the values obtained between $E=-2.47J$ and $E=-2.37J$ with the correlation function. The coherent oscillations are damped at a time $t_d=1/\gamma_{13}$, where γ_{13} is given by Eq. (6). If we retain only the $u=1$ and $u=3$ states in our calculation, the damping constant due to intraband relaxation at low temperature $(k_BT\ll E_3-E_1)$ is approximately $\gamma_{13}\approx\frac{1}{2}\Sigma_n\phi_{1,n}^2\phi_{3,n}^2W_0((E_3-E_1)/J)^3=64W_0\pi^6/(N^*+1)^6$. For $W_0=16$ and $N^*=27$, we obtain $t_d\approx500/J$. The damping observed in our calculated spectra is faster (see Fig. 6) and is affected by inhomogeneous dephasing caused by the limited frequency resolution in our spectra. The resolution is $3.5\times10^{-3}J$, leading to an inhomogeneous dephasing time of $290/J$.

VI. DISCUSSION

This paper discusses the 2D spectrum at low pulse intensities, in which case the nonlinear response functions in Eqs. (8) and (9) can be derived. It is well known that the response depends, in principle, on intensity. With stronger pulses, fifth-order processes, where multiple interactions of the system with the same pulse take place, will contribute more and more to the spectrum.[47] Another well known intensity dependent effect is exciton-exciton annihilation. Our model of monomers as electronic two-level systems does not include the possible existence of states with an energy that is almost resonant with twice the excited state energy. Such states might exist in reality and they provide an efficient radiationless relaxation pathway for two-exciton states. This process has been studied by varying the excitation intensity.[48,49] Because we aim to descibe experiments which use weak pulses, processes that occur at high excitation intensity can be neglected in our treatment. However, because a 2D spectroscopic experiment creates coherent superpositions of two-exciton states with states in the single exciton manifold during t_3, a relaxation of two-exciton states will lead to additional broadening of the induced absorption peak. It would be interesting to study the feasibility of observing the exciton-exciton annihilation process using 2D spectroscopy, even with low pulse intensities.

In our calculations, we have taken a constant value γ for the homogeneous broadening. In principle, the dephasing constant given by Eq. (7) is highly energy dependent. At low temperature, population relaxation from the lowest states in the band is almost impossible, and a dephasing of coherent superpositions of these states and the ground state occurs only by coupling to the electromagnetic field. Because this dephasing is rather slow, homogeneous linewidths at the bottom of the *J*-band are found to be as low as $10^{-4}J$. At energies larger than about $-2.4J$, the dephasing starts to rise quickly and the value of $0.005J$ is found at the top of the *J*-band. Taking into account this variation in the homogeneous linewidth would reduce the antidiagonal width of the diagonal peak. The other peaks have a shape that is determined by inhomogeneous broadening and, therefore, the precise value of γ has little influence. To check the effect of a homogeneous linewidth on the procedure that we used to extract the energy dependent localization length, we have repeated our calculations for different values of γ. We find that it is possible to extract the delocalization length reliably for values of $\gamma\leqslant\gamma_{\mathrm{cr}}=0.012J$. For larger values of γ, the coherence length imposed by a dynamic disorder becomes smaller than the delocalization size,[12] and the latter cannot be obtained from the peak splitting anymore. Our method thus breaks down at higher temperature, first at the blue side of the spectrum. We note that the peak distance does not depend on γ as long as γ is smaller than the critical value. This means that the peak splitting should provide a reliable measure of delocalization size for all energies where the homogeneous broadening is smaller than γ_{cr}. With our parameters, γ_{cr} is found at an energy of $-2.3J$. In commonly studied aggregates, J is in the order of 500–1100 cm^{-1}.[1,44,50,51] The temperature of $k_BT=0.005J$ that we use then corresponds to 3.7–8.3 K. Experiments at temperatures as low as 1.5 K have been reported.[44,52] At these temperatures, it should thus be experimentally possible to find the delocalization length over the whole *J*-band using the proposed method.

We finally comment on the presence of correlation in the site energy disorder. In our calculations, we have modeled the site energies as uncorrelated Gaussian random variables. However, various authors have argued for the presence of correlated disorder in *J*-aggregates.[41,51,53–55] Therefore, we have also calculated the spectra with fully correlated site energies. The site energies of all oscillators in a chain are equal, but there is a distribution of chain energies. This distribution is chosen to be simply Gaussian, with its width chosen to obtain a pump-probe spectrum that looks similar to

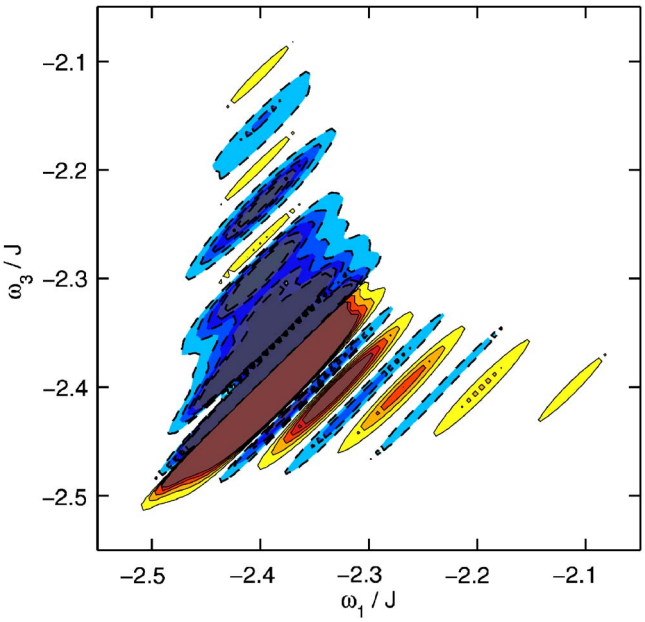

FIG. 7. (Color online) 2D correlation spectra for an alternative disorder model. The spectrum is calculated from an average over homogeneous chains consisting of 100 monomers, but each chain has a different site energy. The chain energy distribution is Gaussian and has a width $0.018J$. The homogeneous width is $0.005J$.

the spectrum for the inhomogeneous chain with $\sigma=0.2J$. In this case, the peaks that are found in the spectrum of a single homogeneous aggregate are seen, but they undergo diagonal broadening, as seen in Fig. 7. The 2D spectra for both disorder models (Figs. 2 and 7) are clearly very different, offering a way to distinguish between the models. However, calculations with finite correlation lengths (not shown) indicate that the effect of correlation is hardly observable if the disorder correlation length is significantly smaller than the exciton coherence length.

VII. CONCLUSION

We have studied the use of 2D optical spectroscopy to extract energy dependent properties of J-aggregates at low temperatures. The combination of the strong diagonal peak with an extended cross peak gives rise to a V shape in the 2D spectrum, on top of which an elliptic positive peak is seen. The broadening caused by thermal dephasing destroys the V shape and its observation is, therefore, characteristic of low temperature aggregates. From an analysis of the main features of the spectrum, one can obtain information on the energy dependence of the exciton localization size. In simulations, the localization size strongly depends on energy. 2D spectroscopy offers a new tool to measure this dependence. In our proposed technique, only the 2D spectrum at zero waiting time is needed. From a numerical simulation, the energy dependent localization length can also be characterized by calculating spatial correlations of the wave function components. We find good agreement between the lengths extracted from the spectrum and the energy dependence of this calculated length and conclude that 2D spectroscopy is a useful tool to measure the energy dependence of the localization length.

2D spectroscopy provides a lot of information on dynamical processes in the manifold of one-exciton states in a multichromophoric system. Relaxation rates at different energies can be obtained, and the 2D spectrum is useful to study coherent superpositions of exciton states. The coherences give clear contributions to the spectrum and inhomogeneous dephasing is, in principle, absent. This makes it possible to study the time evolution of the coherences in detail. Future work should include the energy dependence of the homogeneous linewidth and, for short waiting time, the effects of pulse overlap.

ACKNOWLEDGMENTS

We wish to thank F. W. Wubs for introducing us to the Jacobi–Davidson method, and J. A. Klugkist for discussions on the nature of exciton states. T.l.C.J. acknowledges the Netherlands Organization for Scientific Research (NWO) for support through a VIDI grant.

[1] I. Stiopkin, T. Brixner, M. Yang, and G. R. Fleming, J. Phys. Chem. B **110**, 20032 (2006).
[2] G. S. Engel, T. R. Calhoun, E. L. Read, T. K. Ahn, T. Mančal, Y. C. Cheng, R. E. Blankenship, and G. R. Fleming, Nature (London) **446**, 782 (2007).
[3] M. Cho, H. M. Vaswani, T. Brixner, J. Stenger, and G. R. Fleming, J. Phys. Chem. B **109**, 10542 (2005).
[4] P. Kjellberg, B. Brüggemann, and T. Pullerits, Phys. Rev. B **74**, 024303 (2006).
[5] D. Egorova, M. F. Gelin, and W. Domcke, J. Chem. Phys. **126**, 074314 (2007).
[6] E. L. Read, G. S. Engel, T. R. Calhoun, T. Mančal, T. K. Ahn, R. E. Blankenship, and G. R. Fleming, Proc. Natl. Acad. Sci. U.S.A. **104**, 14203 (2007).
[7] K. Hyeon-Deuk and Y. Tanimura, J. Chem. Phys. **127**, 075101 (2007).
[8] D. Abramavicius, L. Valkunas, and S. Mukamel, Europhys. Lett. **80**, 17005 (2007).
[9] V. Szöcs, T. Pálszegi, V. Lukeš, J. Sperling, F. Milota, W. Jakubetz, and H. F. Kauffmann, J. Chem. Phys. **124**, 124511 (2006).
[10] H. Fidder, J. Knoester, and D. A. Wiersma, J. Chem. Phys. **95**, 7880 (1991).
[11] M. Bednarz, V. A. Malyshev, and J. Knoester, Phys. Rev. Lett. **91**, 217401 (2003).
[12] D. J. Heijs, V. A. Malyshev, and J. Knoester, Phys. Rev. Lett. **95**, 177402 (2005).
[13] A. V. Malyshev, V. A. Malyshev, and J. Knoester, Phys. Rev. Lett. **98**, 087401 (2007).
[14] H. Fidder, J. Knoester, and D. A. Wiersma, J. Chem. Phys. **98**, 6564 (1993).
[15] A. M. van Oijen, M. Ketelaars, J. Köhler, T. J. Aartsma, and J. Schmidt, Science **285**, 400 (1999).
[16] J. Hernando, E. M. H. P. van Dijk, J. P. Hoogenboom, J. J. García-López, D. N. Reinhoudt, M. Crego-Calama, M. F. García-Parajó, and N. F. van Hulst, Phys. Rev. Lett. **97**, 216403 (2006).
[17] L. Valkunas, J. Janusonis, D. Rutkauskas, and R. van Grondelle, J. Lumin. **127**, 269 (2007).
[18] D. B. Chesnut and A. Suna, J. Chem. Phys. **39**, 146 (1963).
[19] G. Juzeliunas, Z. Phys. D: At., Mol. Clusters **8**, 379 (1988).
[20] F. C. Spano, Phys. Rev. Lett. **67**, 3424 (1991).
[21] A. Stathopoulos, SIAM J. Sci. Comput. (USA) **29**, 481 (2007).
[22] A. Stathopoulos and J. R. McCombs, SIAM J. Sci. Comput. (USA) **29**, 2162 (2007).
[23] H. Fidder, Chem. Phys. **341**, 158 (2007).

[24] A. S. Davydov, *Theory of Molecular Excitons* (Plenum, New York, 1971).
[25] M. Bednarz, V. A. Malyshev, and J. Knoester, J. Chem. Phys. **117**, 6200 (2002).
[26] D. J. Heijs, V. A. Malyshev, and J. Knoester, J. Chem. Phys. **123**, 144507 (2005).
[27] D. J. Heijs, A. G. Dijkstra, and J. Knoester, Chem. Phys. **341**, 230 (2007).
[28] R. M. Hochstrasser, Proc. Natl. Acad. Sci. U.S.A. **104**, 14189 (2007).
[29] D. M. Jonas, Annu. Rev. Phys. Chem. **54**, 425 (2003).
[30] S. Mukamel, *Principles of Nonlinear Optical Spectroscopy* (Oxford University Press, Oxford, 2005).
[31] S. M. Gallagher Faeder and D. M. Jonas, J. Phys. Chem. A **103**, 10489 (1999).
[32] M. Khalil, N. Demirdöven, and A. Tokmakoff, J. Phys. Chem. A **107**, 5258 (2003).
[33] J. Knoester, Phys. Rev. A **47**, 2083 (1993).
[34] M. Cho and G. R. Fleming, J. Chem. Phys. **123**, 114506 (2005).
[35] A. V. Malyshev and V. A. Malyshev, Phys. Rev. B **63**, 195111 (2001).
[36] J. Klugkist, V. A. Malyshev, and J. Knoester, J. Lumin. **128**, 945 (2008).
[37] T. Meier, V. Chernyak, and S. Mukamel, J. Phys. Chem. B **101**, 7332 (1997).
[38] M. Dahlbom, T. Pullerits, S. Mukamel, and V. Sundström, J. Phys. Chem. B **105**, 5515 (2001).
[39] M. Schreiber and Y. Toyozawa, J. Phys. Soc. Jpn. **51**, 1537 (1982).
[40] R. Gadonas, R. Danelyus, A. Piskarskas, and S. Rench, Izv. Akad. Nauk SSSR, Ser. Fiz. **47**, 2445 (1983).
[41] J. R. Durrant, J. Knoester, and D. A. Wiersma, Chem. Phys. Lett. **222**, 450 (1994).
[42] M. van Burgel, D. A. Wiersma, and K. Duppen, J. Chem. Phys. **102**, 20 (1995).
[43] Y. Hamanaka, H. Kurasawa, A. Nakamura, Y. Uchiyama, K. Marumoto, and S. Kuroda, Chem. Phys. Lett. **363**, 233 (2002).
[44] J. Moll, S. Daehne, J. R. Durrant, and D. A. Wiersma, J. Chem. Phys. **102**, 6362 (1995).
[45] L. D. Bakalis and J. Knoester, J. Phys. Chem. B **103**, 6620 (1999).
[46] A. V. Pisliakov, T. Mančal, and G. R. Fleming, J. Chem. Phys. **124**, 234505 (2006).
[47] B. Brüggemann, P. Kjellberg, and T. Pullerits, Chem. Phys. Lett. **444**, 192 (2007).
[48] H. Stiel, S. Daehne, and K. Teuchner, J. Lumin. **39**, 351 (1988).
[49] V. Sundström, T. Gillbro, R. A. Gadonas, and A. Piskarskas, J. Chem. Phys. **89**, 2754 (1988).
[50] H. Fidder, J. Terpstra, and D. A. Wiersma, J. Chem. Phys. **94**, 6895 (1991).
[51] I. G. Scheblykin, O. Yu. Sliusarenko, L. S. Lepnev, A. G. Vitukhnovsky, and M. van der Auweraer, J. Phys. Chem. B **105**, 4636 (2001).
[52] H. Fidder, J. Knoester, and D. A. Wiersma, Chem. Phys. Lett. **171**, 529 (1990).
[53] J. Knoester, J. Chem. Phys. **99**, 8466 (1993).
[54] V. A. Malyshev, A. Rodríguez, and F. Domínguez-Adame, Phys. Rev. B **60**, 14140 (1999).
[55] M. Bednarz and P. Reineker, J. Lumin. **119**, 482 (2006).